

## Source Fault Analyses from InSAR Data and Aftershocks for the Fin Doublet Earthquakes on 14 November 2021 in Hormozgan Province, South Iran

Rezapour, M.<sup>1</sup>  | Jamalreyhani, M. R.<sup>2</sup> 

1. **Corresponding Author**, Department of Seismology, Institute of Geophysics, University of Tehran, Tehran, Iran. E-mail: [rezapour@ut.ac.ir](mailto:rezapour@ut.ac.ir)

2. Department of Seismology, Institute of Geophysics, University of Tehran, Tehran, Iran. E-mail: [m.jamalreyhani@ut.ac.ir](mailto:m.jamalreyhani@ut.ac.ir)

(Received: 26 Jan 2022, Revised: 12 June 2022, Accepted: 4 Oct 2022, Published online: 5 March 2023)

### Abstract

The Fin doublet earthquakes with magnitudes  $M_N$  6.2 and 6.3 occurred on November 14, 2021 in Hormozgan province, south of Iran, and were followed by many aftershocks with magnitude range between  $M_N$  2.5 and  $M_N$  5.0. In this study, first we conducted the InSAR analysis using the satellite data from European Space Agency (ESA) to the Fin doublet earthquakes. The displacement field obtained from interferometric observations in ascending and descending directions, exhibit ~E-W oriented pattern reverse fault. Then, we relocated aftershocks that were recorded between November 14, 2021 and January 14, 2022, using the double-difference relocation method (hypoDD). The general pattern of relocated aftershocks distribution shows a seismic zone covering an area of approximately  $25 \times 17$  km<sup>2</sup>. The cross-sections through aftershock locations show that the dominant depth range of aftershocks is from ~4 to ~23 km. The results show that the focal depths decrease toward the northeastern part of the region and deeper-aftershocks are located in the southwestern part. The interferometric observations and distribution of relocated aftershocks suggest the source fault(s) of the Fin doublet earthquakes strikes along a nearly west–east line and dip toward south-to-southeast.

**Keywords:** Fin-Hormozgan, Doublet earthquakes, InSAR, Aftershocks, South of Iran, Relocation, hypoDD.

### 1. Introduction

On November 14, 2021 the Fin  $M_N$  6.2,  $M_N$  6.3 doublet earthquakes occurred in southeastern part of the Zagros Mountains near the northern shore of the Persian Gulf (Figure 1). The magnitude, spatial and temporal proximity of two events acknowledge them like doublet earthquakes. Considering the Iranian Seismological Center (IRSC) catalogue, no foreshock preceded the Fin doublet earthquakes, and they were followed by many aftershocks. The Iranian plateau, including the area of the Zagros Mountain range in which the Fin doublet earthquakes occurred, is one of the intercontinental shortening zones. The shortening in this area is mainly done as detachment folding in which the uppermost sediments may be decoupled from the underlying deformation by mechanically weak layers that act as barriers to rupture (Davis & Engelder, 1985; Mitra, 2003). The 2021 Fin doublet earthquakes provide an opportunity to study the connection between

faulting and folding in the Simply Folding Belt (SFB) in Zagros.

It is well known that the Zagros Mountains originated from the closure of the Neo-Tethys Ocean. The Zagros Fold-Thrust Belt (ZFTB) consists of some parallel major thrust faults including the High Zagros Fault (HZF), the Mountain Front Fault (MFF), and the Zagros Foredeep Fault (ZFF) (Figure 1). The MFF is known as a segmented reverse fault zone characterized by high earthquake activity (Berberian, 1995; Mohammadnia et al., 2018). The ZFF is a border of the alluvial basin of the Zagros in the southwest and the folded belt in the northeast (Berberian, 1995; Sepehr & Cosgrove, 2005; Zamani & Agh-Atabai, 2009). As the dominant tectonic feature of this region, the Arabian plate converges into the Eurasian plate trending north to north-northeast at velocity ranges of the order of 23-25 to 35 mm/year (Berberian, 1976; Jackson & McKenzie, 1984; DeMets et al., 1990; Walker & Jackson, 2002;

Cite this article: Rezapour, M., & Jamalreyhani, M. R. (2023). Source Fault Analyses from InSAR Data and Aftershocks for the Fin Doublet Earthquakes on 14 November 2021 in Hormozgan Province, South Iran. *Journal of the Earth and Space Physics*, 48(4), 87-97. DOI: <http://doi.org/10.22059/jesphys.2022.337959.1007399>



McClusky et al., 2003; Vernant et al., 2004). As shown in Figure 1, the level of seismicity in the study area is high, and several earthquakes with magnitude  $M \geq 5.5$  occur each year in the region.

The surface geology of the Fin region comprises of a series of parallel, E–W trending folds that expose sediments ranging from the Pliocene–Pleistocene Bakhtyari conglomerates down to the Eocene–Oligocene Asmari limestone (Figure 1b). These folds are a mixture of concentric, open structures (e.g. Fin syncline, Guniz & Handun anticlines) and anticlines that verge strongly toward the south, with steepened or even overturned southern limbs (e.g. Anguru & Ginau anticlines). Some of the anticlines such as Guniz, Handun and Tashkend also have exposures of Proterozoic–Cambrian Hormuz salt in their cores (Roustaei et al., 2010).

In this work, first we analyze the InSAR data, then we study the spatial distribution of the aftershock sequence and clarify the activities associated with causative fault(s). We approach to analyze the recorded aftershocks using single-event and multiple-event locating programs. Here, we present the results of analyses using InSAR and aftershocks data, to gain insight into local tectonics, geometry of the rupture zone. The outcome of this study may be useful for evolving a comprehensive earthquake hazard model for the region in the near future.

## 2. InSAR Data Analysis

Satellite synthetic aperture radar (SAR) data can provide detailed and spatially comprehensive ground information, and an interferometric SAR (InSAR) enables us to measure ground deformation and to study various geodynamic phenomena such as earthquakes, subsidence, landslides, etc. with high precision (Massonnet & Feigl, 1998; Bürgmann et al., 2000). We can analyze the detailed source properties by using the high spatial resolution data that provides us with the detailed crustal deformation distribution for moderate-sized earthquakes. In this study, we conducted the InSAR analysis using the satellite data from European Space Agency (ESA) to the Fin doublet earthquakes in Hormozgan province, south of Iran. The

displacement field obtained from interferometric observations in ascending and descending directions. Co-seismic interferogram of the Fin doublet earthquakes on November 14, 2021 obtained from InSAR analysis by SNAP software from ESA with the implemented interferometric phase unwrapping through SNAPHU (Chen & Zebker, 2002) (Figures 2 and 3). The temporal baseline of ascending and descending orbits is 24 and 12 days, respectively. Due to the very close origin time of both  $M_N$  6.2 and  $M_N$  6.3 doublet earthquakes, the interferogram shows cumulative displacement of both events. However, it is possible that the first event does not contribute in the observed signal, due to its smaller magnitude. The observed fringes look like they could be produced with a single fault plane either by a  $\sim$  north-to-northwest dipping reverse fault, or by a  $\sim$  south-to-southeast dipping one. Fringes show the  $\sim$ 15 cm and 25 cm displacement in Satellite Line-of-Sight (LOS) direction. Both ascending and descending interferograms exhibit  $\sim$ W-E oriented pattern reverse fault.

## 3. Single-Event Locations

During November 14, 2021 to February 14, 2022, IGUT has reported 270 events as Fin-Hormozgan sequence with magnitude range between  $M_N$  2.5 and  $M_N$  5.0. where the  $N$  denotes Nuttli that is an  $mb(Lg)$  magnitude scale specifically designed for earthquakes in the eastern United States using 1-s period  $Lg$  amplitudes (Nuttli, 1973). The  $M_N$  scale used by Institute of Geophysics, University of Tehran (IGUT), is the modified  $mb(Lg)$  scale (Rezapour, 2005). IGUT runs the national seismological network and reports  $M_N$  value for recorded events.

It is well known that an inadequate velocity model led to high uncertainties in hypocentral locations. We applied Velesht (Kissling et al., 1994) to obtain a 1-D velocity profile via a joint velocity-hypocenter inversion using Ilaghi et al. (2010) model as an initial model. The result suggests a 12-km-thick layer with  $V_p=5.60$  km/s at the top,  $V_p=6.10$  km/s at depths of 12–20 km, a lower layer with  $V_p=6.40$  km/s to 45 km depth, and a half-space with  $V_p=8.10$  km/s. Also, we used the Kianimehr et al. (2008) model as an initial model and

implemented the VELEST program, the obtained model is not significantly different from the model mentioned above. Using this model and  $V_p/V_s$  ratio of 1.73 the Fin doublet earthquakes and their aftershocks were relocated by the locating program HYPOINVERSE (Klein, 1985; Havskov & Ottemöller, 2005). We used the available data recorded by seismic stations, which are shown in Figure 1 and Table 1. Reported locations for the Fin doublet earthquakes by different seismological agencies are largely different (Table 2). The values in Table 2 are the latest updated values. Determined hypocenters and focal mechanisms for Fin doublet earthquakes by

different seismological centers are plotted in Figure 4. Focal mechanisms, describing the style of faulting for both events, suggest slip on reverse fault striking roughly east-west. The Global Centroid Moment Tensor (GCMT) solutions indicate thrust-faulting mechanism with a focal depth of ~12.0 km for both earthquakes. The GFZ fault plane solutions have similar results compared to the GCMT solutions. The USGS solution for the first earthquake with a focal depth of 9.0 km is completely similar to the GCMT and GFZ solutions, but for the second earthquake USGS determined a reverse mechanism with striking roughly SW-NE or SE-NW.

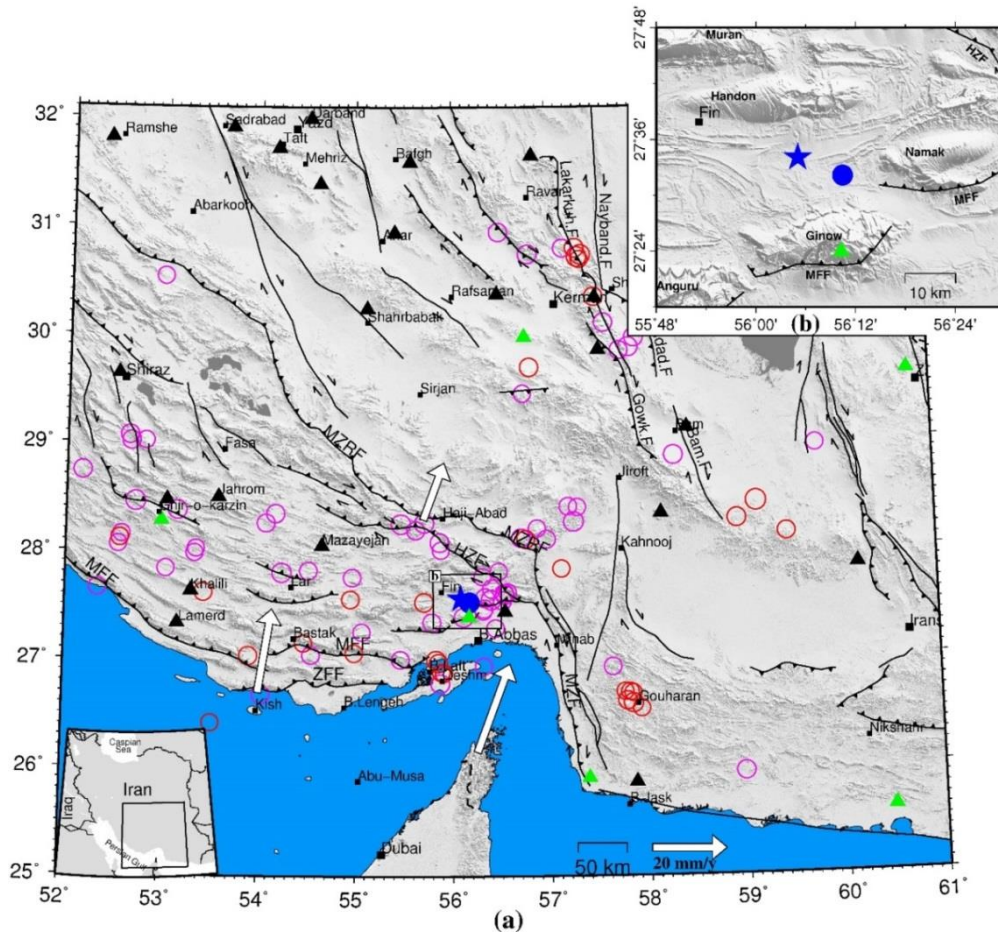


**Figure 1.** (a) Seismicity map of the study area. The open-purple-circles indicate the epicenters of events with magnitudes greater and equal 5.5 (1964-2005), which were extracted from the International Seismological Centre (ISC) bulletin. The open-red-circles show the epicenters of events with magnitude greater and equal 5.5, which occurred in 2006-2021 and were reported by Institute of Geophysics, University of Tehran (IGUT). The blue-star and blue-circle indicate the epicenter of the first and second Fin doublet earthquakes respectively, reported by IGUT. All of the events are scaled according to their magnitude. The solid lines show traces of major active faults in the region. MZR, Main Zagros Reverse Fault; HZF, High Zagros Fault; MFF, Mountain Front Fault; ZFF, Zagros Foredeep Fault; and MZF, Minab Zendan Fault (Hessami et al., 2003; Berberian, 1995). The white-arrows are presenting the GPS velocities relative to stable Eurasia (Vernant et al., 2004). The black and green triangles show the permanent seismic stations, which belongs to the IGUT and International Institute of Earthquake Engineering and Seismology (IIEES), respectively. The location of cities is shown by filled-squares; (b) The topographical map of the Fin region.

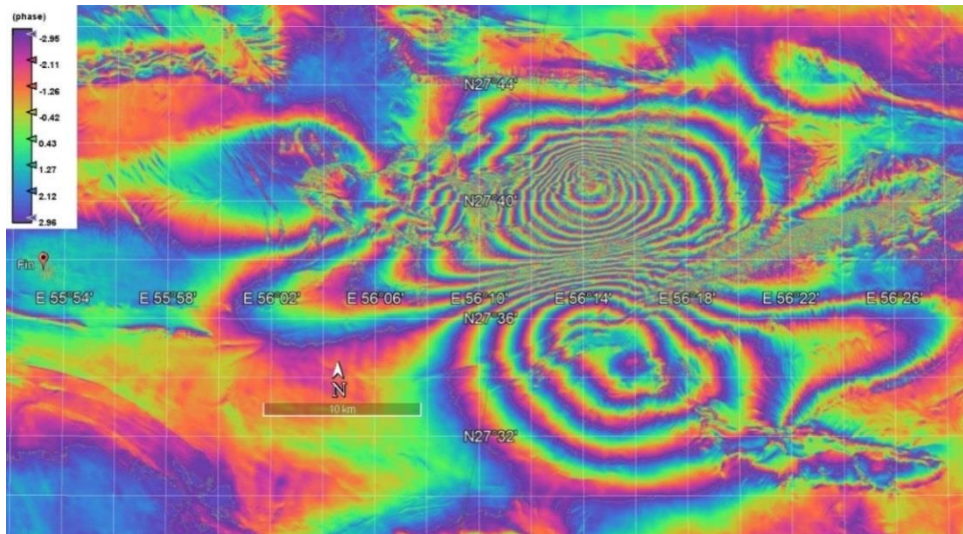


**Figure 2.** Ascending wrapped interferogram from InSAR analysis with temporal baseline of 24 days.

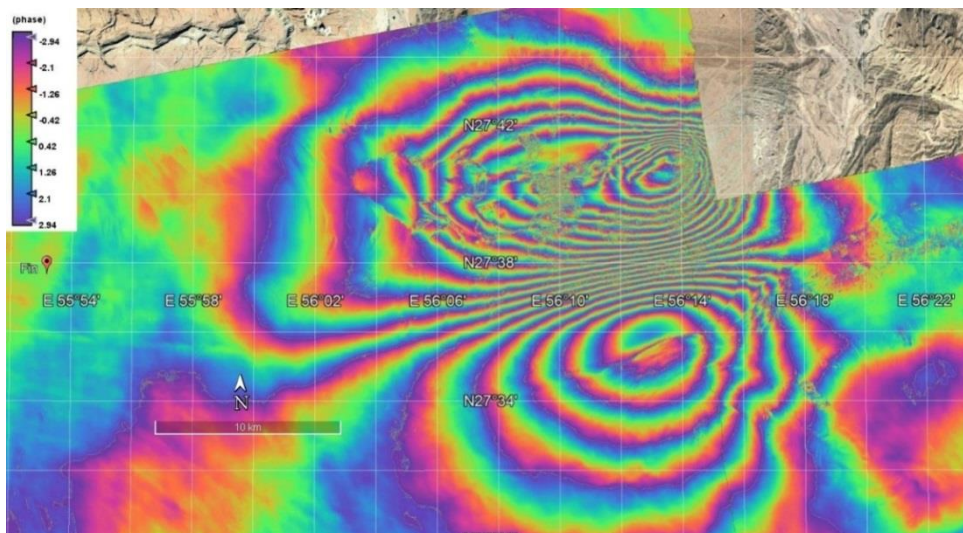


**Figure 3.** Descending wrapped interferogram from InSAR analysis with temporal baseline of 12 days.

**Table 1.** Coordinates of the seismic stations used in this study.

Station Code	Latitude (°)	Longitude (°)	Altitude (m)	Station Owner*	Station Code	Latitude (°)	Longitude (°)	Altitude (m)	Station Owner*
BAF	31.5902	55.5673	1415	IGUT	KHGB	30.3755	56.4768	2057	IGUT
BAZ1	27.8484	60.1869	943	IGUT	KHJ1	28.349	58.1649	889	IGUT
BNB	27.449	56.54	62	IGUT	KHL1	27.6398	53.3007	468	IGUT
BNDS	27.399	56.171	1500	IIEES	KRBR	29.982	56.761	2576	IIEES
BSRN	31.965	59.126	1416	IIEES	KRVR	31.6517	56.8586	1120	IGUT
CHBR	25.595	60.482	125	IIEES	KSHB	30.24118	55.11741	2114	IGUT
CHMN	29.8608	57.5396	2923	IGUT	KSHD	30.3452	57.5125	1150	IGUT
DOBD	31.9903	54.5118	1496	IGUT	LMD1	27.3398	53.1646	425	IGUT
GENO	27.3998	56.1722	1616	IGUT	MEH	31.3899	54.613	1989	IGUT
GHIR	28.286	52.987	1200	IIEES	MZN1	28.0586	54.6517	780	IGUT
JASK	25.8671	57.8663	234	IGUT	QIR1	28.4764	53.0442	740	IGUT
JHRM	28.505	53.577	998	IGUT	RAM	31.8088	52.3815	2000	IGUT
JSSK	25.909	57.387	31	IIEES	SAD	31.9133	53.6854	2464	IGUT
KANR	30.9407	55.4047	1622	IGUT	SHI	29.6374	52.5201	1600	IGUT
KAZ2	29.6128	51.662	884	IGUT	TAFT	31.7228	54.1711	2036	IGUT
KBAM	29.1356	58.4523	971	IGUT	ZHSF	29.611	60.775	1575	IIEES

\* Station owner: IGUT, Institute of Geophysics, University of Tehran; IIEES, International Institute of Earthquake Engineering and Seismology.

**Table 2.** Hypocenter and focal mechanism parameters of the Fin doublet-earthquakes determined by different seismological agencies.

	Agencies*	Origin Time hh:mm:ss.s	Latitude (°)	Longitude (°)	Depth (km)	Magnitude	Strike/Dip/Rake (°)
First-EQ. 2021/11/14	IGUT	12:07:04.4	27.568	56.084	19.5	$M_N$ 6.2	
	IIEES	12:07:04.0	27.668	56.075	14.0	$M_L$ 6.3	
	BHRC		27.65	56.19			
	USGS	12:07:03.0	27.716	56.074	9.0	$M_W$ 6.0	270/63/90 & 91/27/91
	GCMT	12:07:05.5	27.55	56.04	12.0	$M_W$ 6.0	106/35/110 & 262/57/76
	GFZ	12:07:04.5	27.71	56.03	10.0	$M_W$ 6.0	85/28/82 & 273/61/93
	EMSC	12:07:03.8	27.71	56.12	10.0	$M_W$ 6.0	
This study		12:07:04.3	27.575	56.095	20.0	$M_N$ 6.2	
Second E.Q. 2021/11/14	IGUT	12:08:38.1	27.536	56.174	10.0	$M_N$ 6.3	
	IIEES	12:08:36.9	27.565	56.367	15.0	$M_L$ 6.4	
	BHRC		27.69	56.21			
	USGS	12:08:38.0	27.730	56.068	10.0	$M_W$ 6.4	289/85/101 & 41/12/22
	GCMT	12:08:39.9	27.54	56.04	12.9	$M_W$ 6.1	76/25/73 & 275/66/98
	GFZ	12:08:37.5	27.58	56.21	10.0	$M_W$ 6.1	79/28/77 & 273/62/96
	EMSC	12:08:39.0	27.73	56.15	10.0	$M_W$ 6.3	
This study		12:08:38.8	27.576	56.195	9.7	$M_N$ 6.3	

\* Agencies: IGUT, Institute of Geophysics, University of Tehran; IIEES, International Institute of Earthquake Engineering and Seismology; HRC, Building and Housing Research Center; USGS, U.S. Geological Survey; GCMT, Global Centroid Moment Tensor; GFZ, GeoForschungsZentrum, German Research Centre for Geosciences; EMSC, European- Mediterranean Seismological Center.

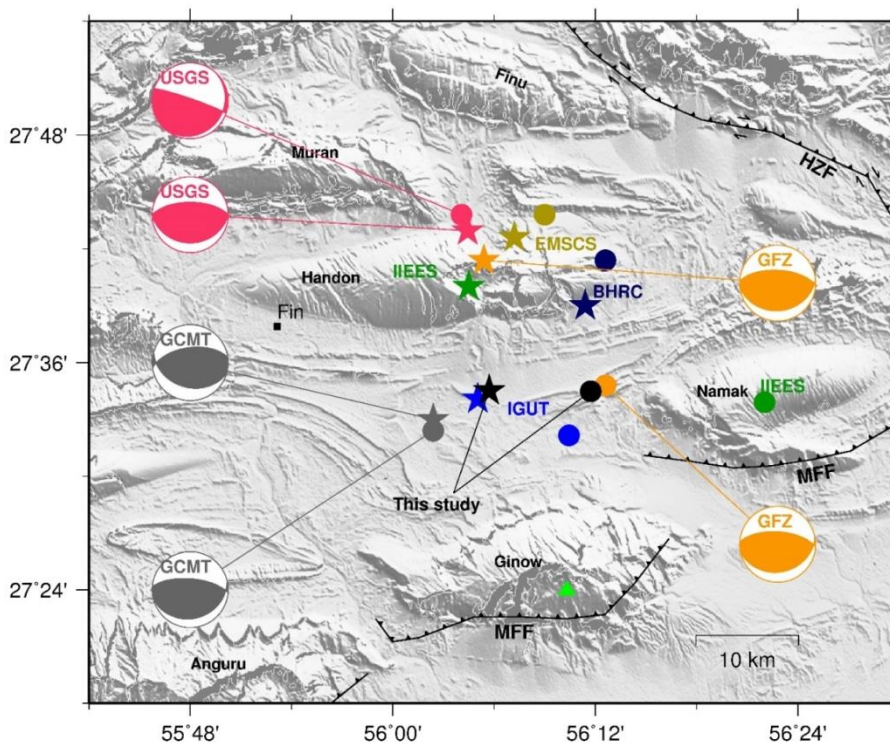


**Figure 4.** Determined epicenters for the first and the second earthquakes on November 14, 2021 are shown by stars and circles, respectively. The focal mechanisms of the doublet-earthquakes are also indicated. Active faults are shown as solid lines: HZF, High Zagros Fault; and MFF, Mountain Front Fault (Hessami et al., 2003; Berberian, 1995). It should be mentioned that the plotted locations correspond to the epicentral coordinates for all agencies except GCMT that corresponds to the centroid. The green-triangle and solid-square represent the BNDS seismic station, which belongs to the IIEES and Fin city, respectively.

Epicentral distribution and three cross sections are plotted in Figure 5, using reported locations by IGUT. Projecting the aftershocks onto profiles in different directions and corresponding normal sections

show that cross sections normal to ~W-E direction well present the causative fault slope. Figure 5b and three cross sections in Figures 5c to 5d show that there is a delineation of aftershocks at focal depth of

10 km, and it seems IGUT has set a fixed depth of 10 km in the location process for about 60 events.

The epicentral distribution and three cross sections are plotted in Figure 6 using relocated date in this study (relocated using hypoinvrse). The confinement of seismicity is mainly between ~4 and ~23 km of the crust (Figure 6b).

Several factors, such as the number of available phases, the station coverage, and the velocity model affect the accuracy of the location. Relative location methods can effectively reduce the uncertainties due to the velocity model and thus give more reliable results (Pavlis, 1992). For applying the relative location method,

we selected a subset data comprising of 204 events with their location uncertainties of  $RMS \leq 0.5$  s,  $ERH \leq 5$  km and  $ERZ \leq 5$  km. Figure 7 shows the histograms of location errors in selected events. Here, the average RMS corresponding to the 204 events is on the order of 0.18 s, and the average location uncertainty in epicenters and depths is about 2.0 km (Figures 7a-7c). Among the location parameters, the depth is normally uncertain. Another important factor controlling the location accuracy at the local scale is network geometry (Bondar et al., 2004; Mottaghi et al., 2010). The average azimuthal gap for the selected data set is  $118.6^\circ$  (Figure 7d).

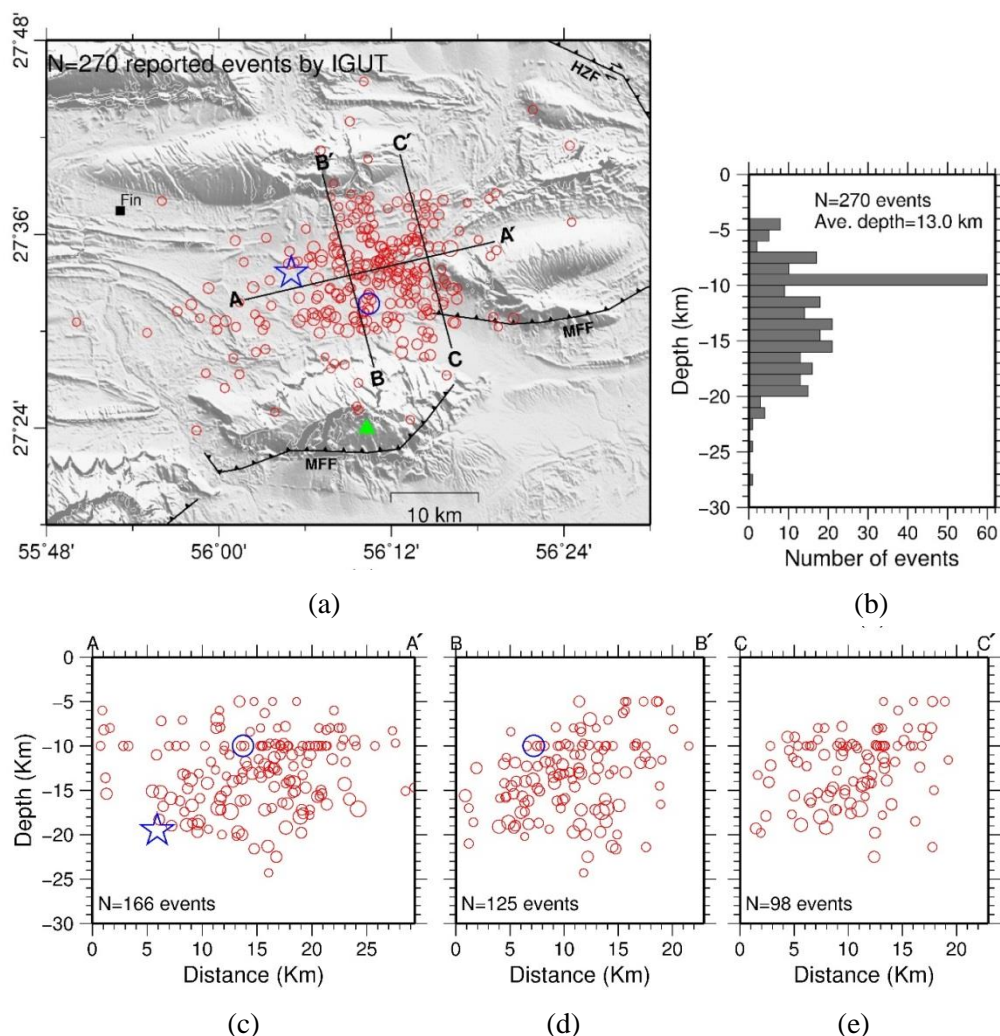


**Figure 5.** (a) Epicentral distribution of 270 events reported by IGUT. The lines A-A', B-B', and C-C' are location lines for sections through the aftershocks illustrated in Figures 5c to 5e; (b) Histogram showing hypocenter depths of 270 events; (c) The section along the strike of the probably causative fault(s); (d) and (e) sections normal to the fault strike. All sections project a 10-km swath of data parallel to the section line. The open-blue-star and open-blue-circle show the locations of the first and second Fin doublet earthquakes, respectively, which occurred on November 14, 2021. The open-red-circles show the location of aftershocks. All of the events are scaled according to their magnitude.

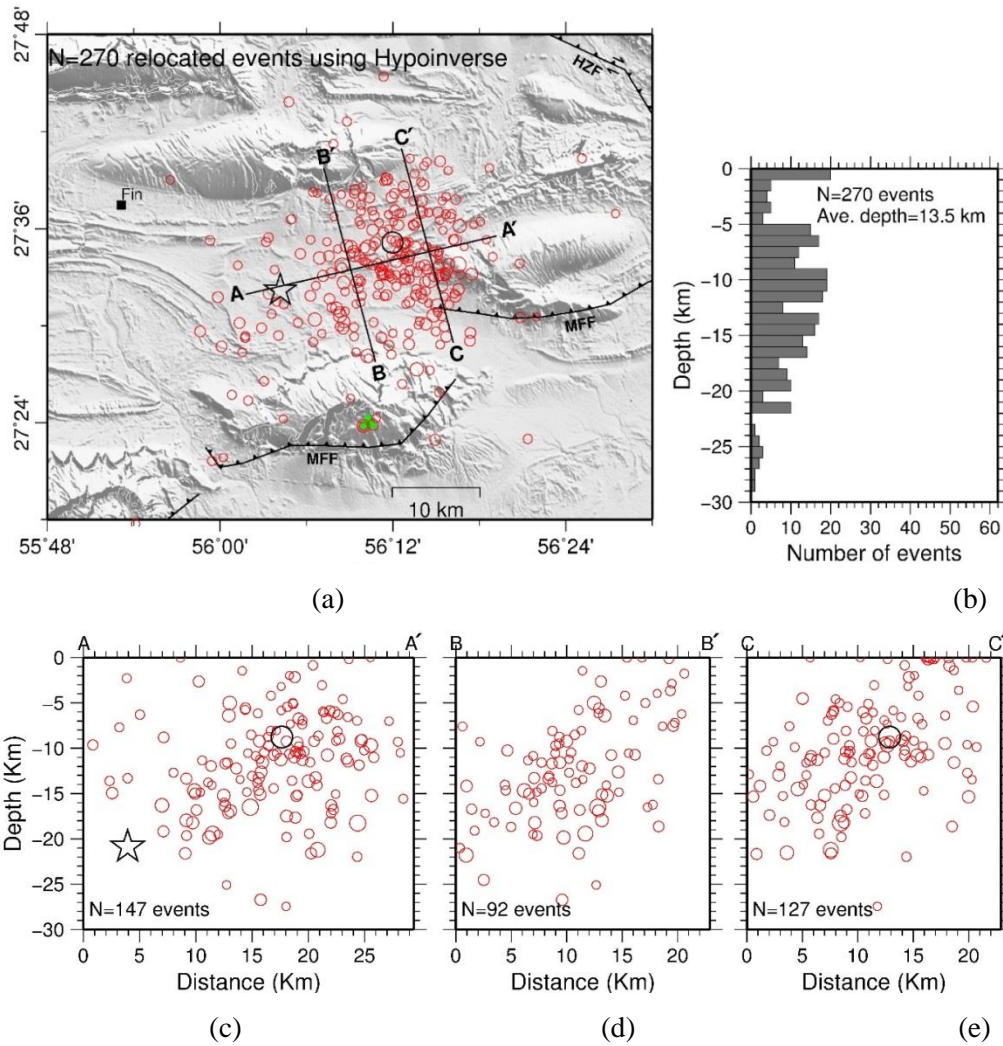


**Figure 6.** (a) Epicentral distribution of 270 events relocated using the single-event method by applying HYPOINVERSE program. The lines A-A', B-B', and C-C' are location lines for sections through the aftershocks illustrated in Figures 4c to 4e; (b) Histogram showing hypocenter depths of 270 events; (c) The section along the strike of the probable causative fault(s); (d) and (e) sections normal to the fault strike. All sections project a 10-km swath of data parallel to the section line. The open-black-star and open-black-circle show the locations of the first and the second Fin doublet earthquakes, respectively, which occurred on November 14, 2021. The open-red-circles show the location of aftershocks. All of the events are scaled according to their magnitude.

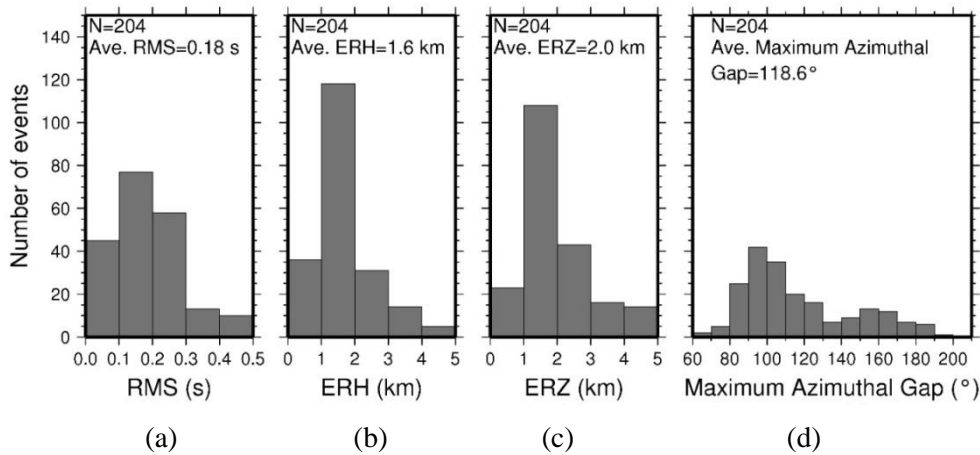


**Figure 7.** Histograms of location uncertainties for 204 subset events relocated using HYPOINVERSE program; (a) The RMS of arrival-time residuals; (b) and (c) are the epicenters and depth uncertainties of the 204 events, respectively; (d) histogram of maximum azimuthal gap of 204 selected events.

### 5. Multiple-Event Locations

To reduce the location uncertainty for closely spaced events such as aftershocks, we used the double-difference method, hypoDD (Waldhauser & Ellsworth, 2000, 2001). The double-difference algorithm has been developed to optimally relocate seismic events in the presence of errors in phase-readings and velocity model uncertainty. In the hypoDD algorithm, the ray paths from two closely spaced events to a common station are assumed similar, and the travel-time residuals at a common station for two events are related to the spatial difference of the two events. The double-difference algorithm has been extensively used for improving the location of aftershocks recorded by permanent or temporary seismic networks. Here, the hypoDD method was applied to relocate 204 selected events from Fin-sequence, and 179 events were successfully relocated.

In general, using the hypoDD technique improves the relative locations, and the amount of improvement mostly depends on the geometry of the seismic network and selected linking parameters. In relocating process, the sensitivity of different parameters such as maximum event-pair separation, minimum observation, and damping factor were carefully investigated for the data set. The hypoDD program reduced the dataset of 204 events to 179 events during the relocation process. The robustness of solutions was tested for subsets of events by using singular value decomposition and randomly changing station distribution. The results show that the hypoDD locations have fairly improved compared to the single-event locations.

### 6. Results and Discussion

In areas like Zagros where seismicity has a diffuse pattern and active basement faults are covered by Phanerozoic sedimentary cover (Berberian, 1976, 1981; Berberian & Tchalenko, 1976; Berberian &

Papastamatiou, 1978), recognition of seismogenic faults is elusive. For the Fin doublet earthquakes, no surface fracture outcrops have been reported. Distribution of 179 relocated aftershock sequences by HypoDD is shown in Figure 8a. Although the surface distribution of the relocated aftershocks does not show a clear trend (Figure 8a), but the interferometric observations show that the fault that caused the doublet Fin earthquakes has probably a west-east strike (Figures 2 and 3). Figure 8a indicates the aftershocks distribution covering an area of approximately  $25 \times 17 \text{ km}^2$ .

Distribution of Fin doublet earthquakes sequence occurred during two months, shows a general view of the causative fault structure for the Fin-Hormozgan earthquakes. To present the fault dip and focal-depth range of the aftershocks, we plot one section approximately parallel to the fault strike and two normal sections in Figures 8d to 8e. These sections project data from a 10-km-wide swath parallel to the section lines. Section A-A' that is approximately parallel to the fault strike shows that the focal depths of the aftershocks are decreased toward the northeastern part (Figure 8c). Sections B-B' and C-C' show that the ruptured zone of the doublet-earthquakes apparently dipping toward south-to-southeast (Figures 8d and 8e).

The Fin doublet earthquakes sequence occurred along complex fault(s) and provided a new constraint on the earthquake hazard in this region. The causative fault was previously unknown, illustrating the difficulty and implications of seismic hazard estimation based on incomplete tectonic maps. Therefore, in Zagros where due to the presence of several ductile layers, capable faults are not easily recognized on the surface, earthquake hazard estimation should not be focused exclusively on identification and study of exposed surface active faults.

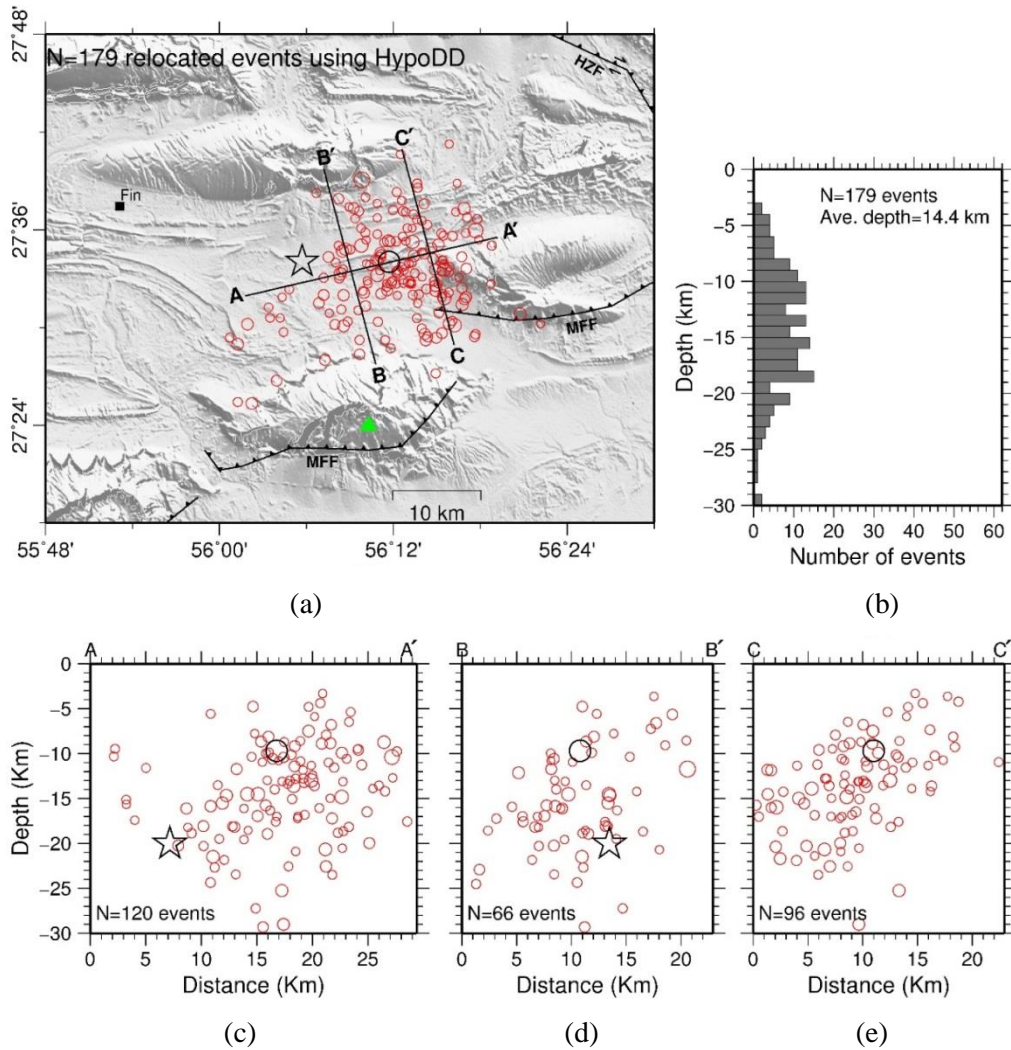


**Figure 8.** (a) Epicentral distribution of 179 events relocated using multi-events method by applying HypoDD program. The lines A-A', B-B', and C-C' are location lines for sections through the aftershocks illustrated in Figures 6c to 6e; (b) histogram showing hypocenter depths of 179 events; (c) the section along the strike of the probably causative fault(s); (d) and (e) sections normal to the fault strike. All sections project a 10-km swath of data parallel to the section line. The open-black-star and open-black-circle show the locations of the first and the second Fin doublet-earthquakes, respectively, which occurred on November 14, 2021. The open-red-circles show the location of aftershocks. All of the events are scaled according to their magnitude.

## 7. Conclusions

The displacement field obtained from interferometric observations in ascending and descending directions using the satellite data from European Space Agency (ESA) to the Fin doublet earthquakes. Both ascending and descending interferograms exhibit ~E-W oriented pattern reverse fault. Also, we analyzed the aftershock sequence of the Fin doublet-earthquakes, which recorded during about two months. The general pattern of relocated aftershocks distribution shows a seismic zone covering an area of approximately  $25 \times 17 \text{ km}^2$ . The sections through aftershock locations show that the

depth range of the aftershocks is from ~4 to ~23 km. The sections through aftershocks show that the aftershocks with large depths are located in the southwestern part of causative fault(s). Therefore, the causative fault striking in ~W-E direction dip toward south-to-southeast.

## Acknowledgments

We acknowledge data supports from the web-sites of Institute of Geophysics, University of Tehran (IGUT), International Institute of Earthquake Engineering and Seismology (IIEES), Building and Housing Research Center (BHRC), International

Seismological Centre (ISC), U.S. Geological Survey (USGS), Global Centroid Moment Tensor (GCMT), German Research Centre for Geosciences (GFZ), and European Mediterranean Seismological Center (EMSC). The Generic Mapping Tools (Wessel & Smith, 1998) was used to graphical representations.

## References

- Berberian, M. (1976). Contribution to the seismotectonics of Iran, Part II (ed. M. Berberian). *Geol. Surv. Iran*, 39, 516 pp.
- Berberian, M. (1981). Active faulting and tectonics of Iran. In: H.K. Gupta and F.M. Delany (Editors), *Zagros-Hindu Kush-Himalaya Geodynamic Evolution. Am. Geophysical. Union, Geodyn. Ser.*, 3, 33-69.
- Berberian, M. (1995). Master blind thrust faults hidden under the Zagros folds—active basement tectonics and surface morphotectonics, *Tectonophysics*, 241, 193–22.
- Berberian, M., & Papastamatiou, D. (1978). Khurgu (North Bandar Abbas, Iran), earthquake of March 21, 1977; a preliminary field report and a seismotectonic discussion. *Bull. Seism. Soc. Am.*, 68, 411-428.
- Berberian, M., & Tchalenko, J. (1976). Earthquakes of the southern Zagros (Iran): Bushehr region. *Geol. Surv. Iran*, 39, 343-370.
- Bondar, I., Myers, S., Engdahl, E., & Bergman, E. (2004). Epicentre accuracy based on seismic network criteria, *Geophys. J. Int.* 156, 483–496.
- Bürgmann, R., Rosen, P. A., & Fielding, E. J. (2000). Synthetic Aperture radar interferometry to measure Earth's surface topography and its deformation, *Annu. Rev. Earth Planet. Sci.*, 28, 169–209.
- Chen C. W., & Zebker, H. A. (2002). Phase unwrapping for large SAR interferograms: Statistical segmentation and generalized network models, *IEEE Transactions on Geoscience and Remote Sensing*, 40, 1709-1719.
- Davis, D.M., & Engelder, T. (1985). The role of salt in fold-and-thrust belts, *Tectonophysics*, 119, 67–88.
- DeMets, C., Gordon, R. G., Argus, D. F., & Stein, S. (1990). Current plate motions, *Geophys. J. Int.* 101, 425–478.
- Havskov, J., & Ottemöller, L. E. (2005). SEISAN: The earthquake analysis software for Windows, SOLARIS, LINUX and MACKINTOSH, Version 8.1, Manual, *Department of Earth Science, University of Bergen, Norway*.
- Hessami, K., Jamali, F., & Tabassi, H. (2003). Major active faults of Iran, scale 1:25,000,000. Ministry of Science, Research and Technology, *International Institute of Earthquake Engineering and Seismology, Iran*.
- Ilaghi, H., Yamini-Fard, F., & Tatar, M. (2010). Crustal velocity structure in Fin region (Zagros - Iran), *J. Earth and Space Physics*, 37, 57-69.
- Jackson, J., & McKenzie, A. D., (1984). Active tectonics of the Alpine-Himalayan belt between western Turkey and Pakistan, *Geophys. J. Res. Astron. Soc.*, 77, 185–264.
- Kianimehr, H., Kissling, E., Yaminifard, F., & Tatar, M. (2018). Regional minimum 1-D P-wave velocity model for a new seismicity catalogue with precise and consistent earthquake locations in southern Iran, *J. Seismol.*, doi:10.1007/s10950-018-9783-4.
- Kissling, E., Ellsworth, W. L., Eberhart-Phillips, D., & Kradolfer, U. (1994). Initial reference models in local earthquake tomography, *J. Geophys. Res.* 99, no. B10, 19635–19646, doi: 10.1029/93JB03138.
- Klein, F. W. (1985). Users guide to HYPOINVERSE, a program for VAX and Professional 350 computers to solve for earthquake locations, *U.S. Geol. Surv. Open-File Rept.* 85-515, 53 pp.
- Massonnet, D., & Feigl, K. L., (1998). Radar interferometry and its application to changes in the earth's surface, *Rev. Geophys.*, 36, 441–500.
- McClusky, S., Reilinger, R., Mahmoud, S., Ben Sari, D., & Tealeb, A. (2003). GPS constraints on Africa (Nubia) and Arabia plate motions, *Geophys. J. Int.*, 155, 126–138.
- Mottaghi, A. A., Rezapour, M., & Yaminifard, F. (2010). Double-difference relocation of earthquake hypocenters along the southern flank of the central Alborz, Iran, *Bull. Seism. Soc. Am.*, 100,

- 2014–2023, doi: 10.1785/0120090147.
- Mitra, S. (2003). A unified kinematic model for the evolution of detachment folds, *J. Struct. Geol.*, 25, 1659–1673.
- Mohammadnia, S., Abbassi, M., Javan-Doloei, G., & Azqandi, M. (2018). Focal mechanism of Mountain front fault (MFF) at a longitude of 46 to 48.5 Degree, *Iranian Journal of Geophysics*, 11, 4, 93–106.
- Nuttli, O. W. (1973). Seismic wave attenuation and magnitude relations for eastern North America, *J. Geophys. Res.* 78, 876–885.
- Pavlis, G. L. (1992). Appraising relative earthquake location errors, *Bull. Seism. Soc. Am.*, 82, 836–859.
- Sepehr, M., & Cosgrove, J.W. (2005). Role of the Kazerun Fault Zone in the formation and deformation of the Zagros Fold-Thrust Belt, Iran. *Tectonics*, 24, TC5005, doi:10.1029/2004TC001725
- Rezapour, M. (2005). Magnitude scale in the Tabriz seismic network, *J. Earth and Space Phys.*, 31, 13–21.
- Roustaei, M., Nissen, E., Abbassi, M., Gholamzadeh, A., Ghorashi, M., Tatar, M., Yamini-Fard, F., Bergman, E., Jackson, J., & Parsons, B. (2010), The 2006 March 25 Fin earthquakes (Iran)—insights into the vertical extents of faulting in the Zagros Simply Folded Belt, *Geophys. J. Int.* 181, 1275–1291. doi: 10.1111/j.1365-246X.2010.04601.x
- Vernant, Ph., Nilforoushan, F., Hatzfeld, D., Abbasi, M. R., Vigny, C., Masson, F., Nankali, H., Martinod, J., Ashtiani, A., Bayer, R., Tavakoli, F., & Chéry, J. (2004). Contemporary crustal deformation and plate kinematics in Middle East constrained by GPS measurements in Iran and northern Oman, *Geophys. J. Int.*, 157, 381–398.
- Waldhauser, F., & Ellsworth, W.L. (2000). HypoDD—A program to compute double-difference earthquake location algorithm: Method and application to northern Hayward fault, California, *Bull. Seism. Soc. Am.*, 90, 1353–1368.
- Waldhauser, F., & Ellsworth, W.L. (2001). HYPODD—A program to compute double-difference hypocenter locations, version 1.0. Open-File Report, *U.S. Geologic Survey*, 01–11325.
- Walker, R., & Jackson, J. (2002). Offset and evolution of the Gowk fault, SE Iran: A major intra-continental strike slip system, *J. Struct. Geol.* 24, 1677–1698.
- Wessel, P., & Smith, W.H.F. (1998). New, improved version of Generic Mapping Tools released, *Eos Trans. AGU.*, 79, 579 pp.
- Zamani, A., & Agh-Atabai, M. (2009). Characteristics of seismicity in the Alborz and Zagros regions of Iran, using a multifractal approach, *Journal of Geodynamics*, 47, 271–279.